

Porous CrO_2 : a ferromagnetic half-metallic member in sparse hollandite oxide family

Sujoy Datta*

Department of Physics, University of Toronto, 60 Saint George Street, Toronto, Ontario M5S 1A7, Canada and
Kadihati KNM High School, Ganti, Kolkata 700135, India[†]

(Dated: September 13, 2024)

A stable polymorph of CrO_2 is predicted using PBE+U method. The porous material is isostructural with $\alpha\text{-MnO}_2$ making it the second transition metal oxide in sparse hollandite group of materials. However, unlike the anti-ferromagnetic semiconducting character of the $\alpha\text{-MnO}_2$, it is found to be a ferromagnetic half-metal. At Fermi level, the hole pocket has ample contribution from O-2p orbital, though, the electron pocket is mostly contributed by Cr-3d_{xy} and Cr-3d_{x²-y²}. A combination of negative charge transfer through orbital mixing and extended anti-bonding state near Fermi level is responsible for the half-metallic ferromagnetic character of the structure. A comparative study of rutile and hollandite CrO_2 and hollandite MnO_2 structures delineate the interplay between structural, electronic and magnetic properties. The material shows a robust magnetic character under hydrothermal pressure, as well as, the band topology is conserved under uniaxial strain. Moderate magneto-crystalline anisotropy is observed and it shows a correspondence with the anisotropy of elastic constants. Occurrence of type-II Weyl nodes and their evolution under pressure is explored.

I. INTRODUCTION

In the field of material science, studies on transition metal oxides (TMO) is prolific. However, TMOs never get tired to amaze the scholars through their versatile character. Not only that, even the burgeoning development in first-principles electronic-structure schemes faces the challenge of describing the underlying Physics of TMOs. Beside dynamical mean free theory (DMFT), inclusion of Hubbard parameters is established as a successful approach in describing TMOs.

Though TMOs are found to form solid-state structure of various symmetries, some structures are known for their uniqueness. The porous layered hollandite structure of $\alpha\text{-MnO}_2$ is such an example [1]. The 2×2 tunnel within this structure can accommodate additional atomic species (e.g., Pb^{2+} , B^{2+} , K^+ , etc.) while producing [2, 3]. Not only it is beneficial for ion storage application for battery industry, but also such additional species can tune the electronic and magnetic properties as well [4–8]. A good number of publications in this field is the testimonial to the importance of study on this structure [7, 9–15]. However, till date, there is no report on any other hollandite TMO exhibiting similar structure with hollow tunnel except $\alpha\text{-MnO}_2$.

Beside Manganese, hollandite oxide structures of Vanadium, Chromium, Ruthenium and Titanium were theoretically or experimentally studied where different cations occupy the tunnel space [16–20]. For example, in $\text{K}_2\text{V}_8\text{O}_{16}$ Potassium ions reside at the tunnel of the hollandite-type structure exhibiting anti-ferromagnetic (AFM) insulating ground state [21, 22]. In contrast $\text{K}_2\text{Cr}_8\text{O}_{16}$ has ferromagnetic (FM) insulat-

ing ground state ($T(95\text{K})$) and, in the temperature range $95\text{K} < T(180\text{K})$ it is found in metallic FM state [23–26].

In $\text{K}_2\text{Cr}_8\text{O}_{16}$, there are two Cr^{3+} and six Cr^{4+} per formula unit. As Cr^{3+} is more stable ionic state found in several compounds, the extraction of K^+ ion is a challenging task. Using electrochemical oxidation or soft-chemistry reactions, partial de-insertion of K^+ have been reported. This may provide a clue to mitigate the hindrance in synthesising porous hollandite CrO_2 [27].

In transition metal family, Chromium is one of its kind. Even at room temperature, is found to be anti-ferromagnetic, making it the only single elemental AFM solid [28]. It shows a valency in the range of [+1 to +6] and oxidize to form CrO , Cr_2O_3 , CrO_2 and CrO_5 . Experimentally, two phases of Chromium dioxides have been characterised, the rutile type (namely $\alpha\text{-CrO}_2$, or, r- CrO_2) and orthogonal CaCl_2 type (namely $\beta\text{-CrO}_2$, or, o- CrO_2). There is a second order phase transition observed from rutile to CaCl_2 type phase at $12\text{--}17\text{ GPa}$ [29, 30]. Some other dynamically stable phases have also been proposed theoretically though hollandite structure have not been predicted yet [31–33].

Transition metals are characterised by the electrons in their d-orbital. In its 4+ valance state, Cr ion has two 3d electrons and a vacant 4s shell. These two 3d electrons should reside at two t_{2g} orbitals. Strong on-site correlation between these two electrons should result in Mott type insulating nature, however, this is not the case. Rutile type Chromium dioxide is a ferromagnetic half-metal at its ground state [34]. An explanation of the half-metallic ferromagnetic character has been provided in terms of the double-exchange model [35–37]. This makes r- CrO_2 a negative charge transfer insulating materials in the Zaanen-Sawatzky-Allen (ZSA) scheme [35, 38]. The O-2p bands crossing the Fermi energy works as a charge (electron/hole) centre to nullify the strong electron-electron correlation between Cr-3d electrons through the hybridisation. Recently the topologi-

* sujoydatta13@gmail.com, sujoy.datta@utoronto.ca

[†] present address.

cal character of rutile and orthorhombic type CrO_2 are investigated. It is shown that type-I and type-II Weyl fermions, can emerge in these phases of chromium dioxide [39].

With the technological advancement, energy storage is a bottleneck yet to be cleaned. Holey structures are efficacious candidate in storing Lithium, Sodium, Zinc or other ions prospective to battery material [40, 41]. Both Chromium and oxygen are abundant in nature, so, h-CrO_2 can be a good alternative in this field. Furthermore, half-metallic ferromagnets are playing a critical role in modern spintronics devices; from magnetic sensors, spin valves to computer hardware components such as magneto-resistive random-access memory (MRAM), read head of magnetic hard drive, etc. [42–45].

In view of the rare ferromagnetic nature of CrO_2 in the TMO family, an investigation on the structures and their local bonding characteristics is indispensable. The aim of this article is to use the latest reliable theoretical approaches to demonstrate the mechanical, electronic and magnetic character of the proposed hollandite polymorph. To analyse and interpret the complicated electronic structures of TMOs, introduction of Hubbard term for both of on-site and off-site electron-electron interaction proved to be an efficacious tool [31, 46].

A detailed side by side investigation of the three materials, already synthesised r-CrO_2 , h-MnO_2 , and the proposed h-CrO_2 can bridge the gap of theoretical understanding on such materials having structural intricacies as well as rich electronic and magnetic properties. Such trustworthy theoretical predictions will facilitate experimentalists a better handle on choosing their materials for a desired application, out of a plethora of possibilities.

II. COMPUTATIONAL DETAILS

We have used the Vienna Ab-initio Simulation Package (VASP) package for density functional theoretical (DFT) calculations [47]. Projected augmented wave (PAW) basis enabled pseudo-potentials using Perdew-Burke-Ernzerhof (PBE) and PBE for solids (PBEsol) generalised gradient approximated (GGA) exchange-correlation (xc) functional have been used [48, 49]. The optimised structures are found through ionic and volume relaxations using GGA and GGA+U methods starting from different magnetic configurations. We have set the threshold of maximum force as 10^{-5} Ry./atom and pressure threshold as $10^{-5} \text{ Kbar/cell}$. The convergence criteria for energy and charge densities has been set as 10^{-8} Ry. We have chosen kinetic-energy cut-off 520 Ry. Fine reciprocal-space grids of dimensions $8 \times 8 \times 8$, $5 \times 5 \times 8$, $5 \times 5 \times 8$ are used for hollandite, rutile and orthorhombic structures, respectively.

The electron configurations of Cr and O have been taken as $[\text{Ar}]4s^23d^4$ and $[\text{He}]2s^22p^4$. As $3d$ electrons of transition metals correlate more strongly than the limit

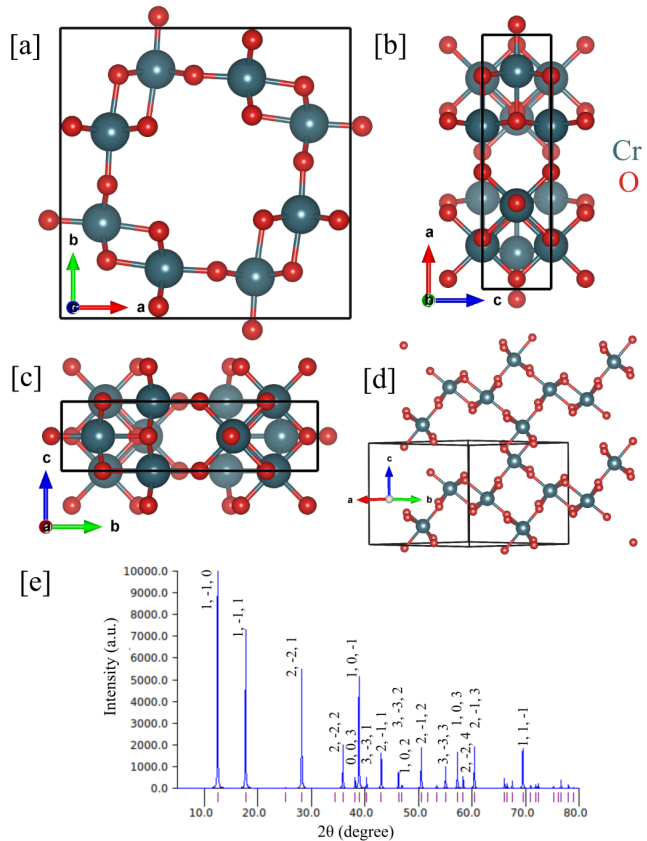


FIG. 1. (a-c) Conventional unit cell of h-CrO_2 crystal having $I4/m$ symmetry, (d) Primitive unit cell, (e) Simulated X-ray Diffraction intensity in arbitrary unit with incident angle for h-CrO_2 .

of GGA, for proper description of strong electron-electron correlation, Hubbard U and Hund J terms have been used. While U provides intra-orbital Coulomb interaction, $U - J$ takes care of the inter-orbital Coulomb interaction between electrons.

Over the years, several non-empirical approaches have been proposed to estimate Hubbard parameters, such as constrained DFT, constrained random phase approximation (cDFT/cRPA) and linear-response formulation [50, 51]. These terms for r-CrO_2 have been calculated by constrained screening method by Korotin *et al.* [35]. We have used these values for CrO_2 : $U = 3.0$ and $J = 0.87$. For MnO_2 , $U = 5.87$ is used [52].

The Vesta package has been utilised to simulate X-ray diffraction (XRD) pattern for Cu_α radiation [53]. For pre and post-processing Vaspkit and ElATools are utilised [54, 55]. The chemical bonding analysis has been done using Lobster package for PAW [56].

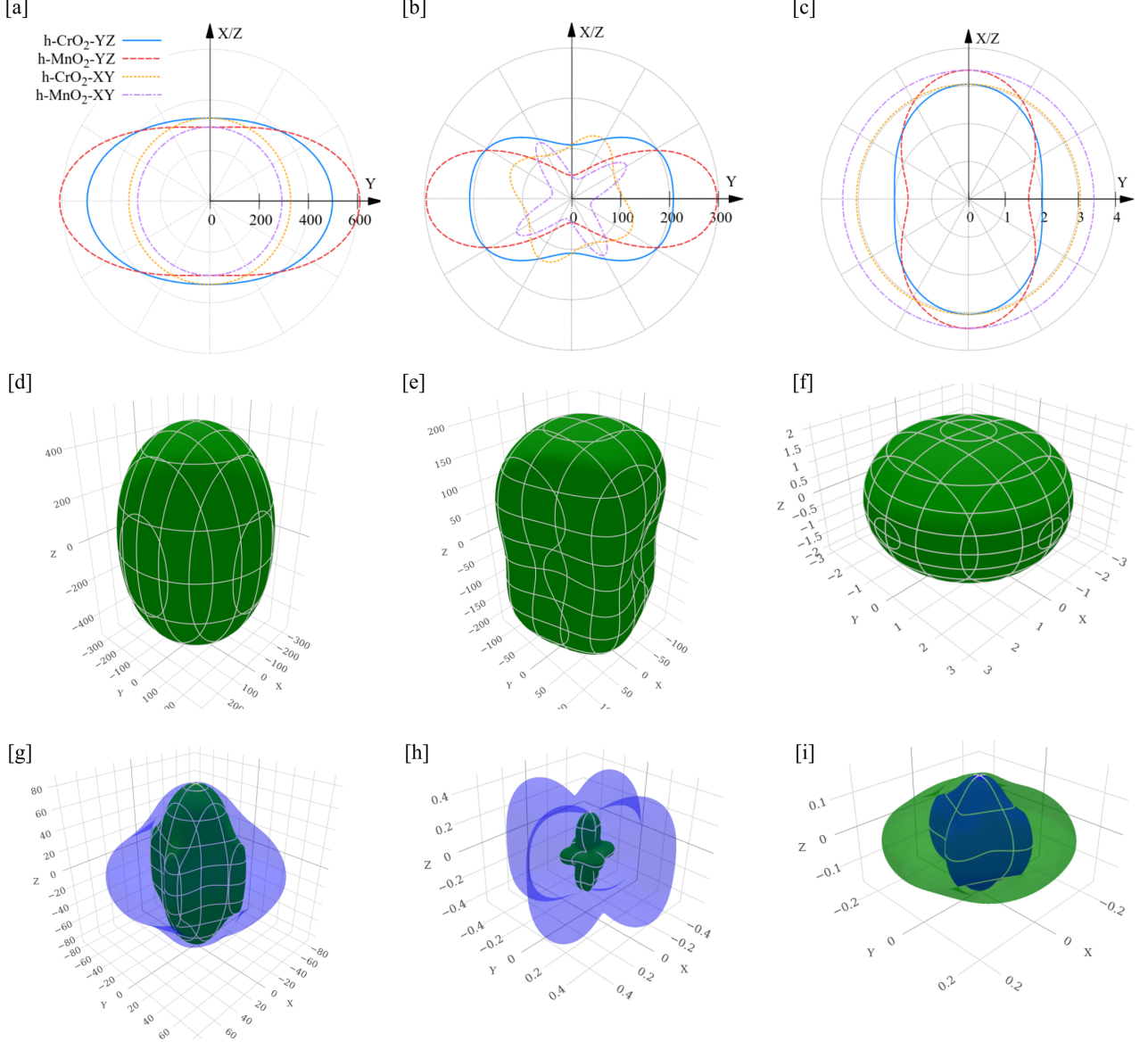


FIG. 2. (a) Bulk modulus (GPa), (b) Young modulus (GPa), (c) Compressibility (1/TPa) in XY and YZ plane of h-CrO₂ and h-MnO₂; Three dimensional plot of (d) Bulk modulus (GPa), (e) Young modulus (GPa), (f) Compressibility (1/TPa), (g) Shear modulus (GPa), (h) Poisson ratio, (i) Inverse Pugh ratio (G/B_H) of h-CrO₂.

III. STRUCTURE AND MECHANICAL PROPERTIES

The hollandite [57] CrO₂ follows body-centred tetragonal lattice having I4/m (82) crystal symmetry. The optimised lattice constants are found to be $a = b = 9.992\text{\AA}$ and $c = 2.702\text{\AA}$ calculated using PBE for spin unpolarised calculation. As depicted in Fig.1 (a-c), the Cr atoms coordinate with six neighbouring oxygen atoms forming edge-sharing CrO₆ octahedra. Such MO₆ type structure is also found in the rutile CrO₂ and is a com-

mon building block for many covalently bonded hard materials [58]. A 2×2 tunnel is formed in between the CrO₆ octahedra. Including Hubbard terms $U = 3.0$ and $J = 0.87$ with PBE exchange-correlation the optimised lattice parameters are calculated as $a = b = 9.880\text{\AA}$ and $c = 2.978\text{\AA}$ [35]. So, there is a relative underestimate of the volume by 7.23% by the unpolarised calculation. Using same Hubbard parameters and PBEsol the lattice constants are found as $a = b = 9.767\text{\AA}$, $c = 2.928\text{\AA}$.

In Fig.1(a-c), the conventional unit cell of h-CrO₂ crystal having eight formula units is shown

from different angles. The primitive cell used for electronic structure calculations is presented in Fig.1(d). The primitive cell contains four formula units. Now, for experimental identification of any crystal structure, XRD spectra is the key. Here in Fig.1(e), we provide the XRD spectra for Cu_α radiation. Reflection from (1,1,0), (1,1,1), (2,2,1) and (1,0,-1) crystallographic planes create the most prominent sharp peaks of XRD. This represents the signature character of the particular structure.

Experimentally two polymorphs of CrO_2 are prepared so far, the rutile type $\alpha\text{-CrO}_2$ (or $r\text{-CrO}_2$) and orthorhombic $\beta\text{-CrO}_2$ (or $o\text{-CrO}_2$). The lattice constants for both these structures predicted using PBEsol+U are agreeing with the experimental findings (see, Table-I).

The hollandite structure of MnO_2 is known as $\alpha\text{-MnO}_2$. The calculated lattice constants for conventional unit cell using PBEsol+U are $a = b = 9.787\text{\AA}$ and $c = 2.903\text{\AA}$ match well with the reported experimental values $a = b = 9.750\text{\AA}$ and $c = 2.861\text{\AA}$ [59].

Elastic properties: Within elastic limit, according to Hook law, the stress (σ_i) and external strain (e_j) follow a linear relationship: $\sigma_i = \sum_{j=1}^6 C_{ij} e_j$, where, C_{ij} is the elastic stiffness tensor. The orthorhombic system has nine independent components in the 6×6 matrix. The rutile structure being a part of type-I tetragonal system possesses six independent components. The hollandite structure which falls under type-II tetragonal class possesses seven independent components. Beside the stress-strain relationship, the elastic tensor can also be calculated from the total energy (E) using the harmonic approximation as: $C_{ij} = \frac{1}{V_0} \frac{\partial^2 E}{\partial e_i \partial e_j}$, where, V_0 is the volume without any stress. The values of C_{ij} are tabulated in Table I.

While all other structures are experimentally reported, $h\text{-CrO}_2$ is not been synthesised yet. Hence, a mechanical stability check is indispensable. Following the Born stability criteria extended to different crystal classes, the necessary and sufficient conditions for mechanical stability (Eq. 1) are satisfied by all the structures are [62, 63]:

$$\begin{aligned} &\text{Orthorhombic: } C_{11}, C_{44}, C_{55}, C_{66} > 0; C_{11}C_{22} > C_{12}^2; \\ &C_{11}C_{22}C_{33} + 2C_{12}C_{13}C_{23} - C_{11}C_{23}^2 - C_{22}C_{13}^2 - C_{33}C_{12}^2 > 0 \\ &\text{Tetragonal-I: } C_{11} > |C_{12}|, C_{44}, C_{66} > 0; \\ &2C_{13}^2 < C_{33}(C_{11} + C_{12}) \\ &\text{Tetragonal-II: } C_{11} > |C_{12}|; C_{44} > 0; \\ &2C_{13}^2 < C_{33}(C_{11} + C_{12}); 2C_{16}^2 < C_{66}(C_{11} - C_{12}) \end{aligned} \quad (1)$$

Beside the elastic stability of the proposed material, its dynamical stability test is necessary. As the vibrational modes (phonons) generate due to the relative kinetics of ions, for a dynamical stable structure, there should be no negative phonon mode. The phononic energy dispersion in Fig.A.1(a) delineate the dynamical stability. Chromium ions (Cr^{4+}) are much heavier than oxygen ions (O^{2-}), therefore, the lower energy phononic modes are populated by the contribution from Cr. Optical modes of higher frequency are mostly contributed by the kinetics of Oxygen ions.

The resistance against the external compression reflects in the bulk modulus of material. Using the Voigt-Reuss-Hill methodology the bulk moduli (B_H) are calculated [60, 64, 65]. A set of separate calculation has been carried out to find the variation of energy with changing volume. The equation of state (EOS) fittings for those data provide another set of bulk moduli. In Table-I B_V represent the bulk moduli calculated using Vinet EOS [66]. The calculated B_V using PBEsol+U for $r\text{-CrO}_2$ is in line with the experimental value [29]. From literature, the theoretically predicted values of the bulk modulus for $r\text{-CrO}_2$ are found as 261 GPa [31], 282 GPa [67], 225 GPa [68], 238 GPa [69]. Now, there is a mismatch of theoretical and experimental bulk moduli of $o\text{-CrO}_2$ structure (216.75 vs. 181). Maddox *et al.* have suspected that as the orthorhombic phase is not found in ambient pressure, the zero pressure volume can not be measured experimentally [29]. Therefore, an effect of inadequate data may results in the EOS prediction for the phase.

Along with the Young moduli (Y), the shear moduli (G), Poisson ratios (ν), Pugh ratios (B_H/G) are calculated using the same Voigt-Reuss-Hill methodology and are tabulated in Table-I. Relative to the orthorhombic and rutile structures, the hollandite structure has large vacuum present in between the CrO_6 polyhedra giving more space to accommodate the the deformation produced by external strains. As a result, B, Y and G values of of the $h\text{-CrO}_2$ phase are much less than other polymorphs. The 2×2 tunnel is also present in $h\text{-MnO}_2$, so, the values of elastic moduli come out to be almost similar to those ones of $h\text{-CrO}_2$.

As for tetragonal class of materials the elastic constants follow the relation: $C_{12} = C_{21}$, hence, the variation of bulk moduli in the XY plane for both $h\text{-CrO}_2$ and $h\text{-MnO}_2$ are isotropic in nature, whereas, in ZX or ZY plane they show elliptical variation as depicted in Fig.2 (a). The eccentricity of the variation in ZY plane is lower for $h\text{-CrO}_2$, while, the bulk modulus in XY plane is higher for the same. In contradiction to $h\text{-CrO}_2$, YZ plot of bulk modulus of $h\text{-MnO}_2$ shows a dip at $Z = 0$. The variation of compressibility in Fig.2(c) is a confirmation of the fact that higher bulk modulus yields less compressibility. According to the Young moduli in Fig. 2(b), $h\text{-CrO}_2$ is less stiff along Z direction than $h\text{-MnO}_2$. The anisotropy of the elastic moduli can be visually confirmed through Fig.2(d-e). In XY plane, the pattern of Young modulus shows it is hard to deform the shape of the 2×2 tunnel in $h\text{-CrO}_2$. As $h\text{-MnO}_2$ is found in AFM ground state, its resistance against the displacement of Mn atoms is more robust.

IV. ELECTRONIC STRUCTURE

The electronic structure and magnetic behaviour of CrO_2 has always been a curious case. While it is more likely for an TMO to be found in anti-ferromagnetic character, CrO_2 is found to be ferromagnetic in its ground state. For anti-ferro spin configuration we have taken three different arrangements as depicted in Fig.3(a-c). The EOS plot confirms the ferromagnetic ground state of $h\text{-CrO}_2$. The AFM-1 state is 30 meV/atom higher in energy than the FM configuration. The AFM-1 and AFM-2 states are very close in energy, and for a range of external pressure it is showing a crossover. However, the ferromagnetic ground state remains stable under pressure, which indicates robustness of magnetic

Material	Method	Lat. Cnst.(Å)	Elastic Const. (GPa)										B_H (GPa)	B_V (GPa)	Y (GPa)	G (GPa)	ν	$\frac{B_H}{G}$
			C_{11}	C_{22}	C_{33}	C_{44}	C_{55}	C_{66}	C_{12}	C_{13}	C_{23}	C_{16}						
r-CrO ₂	PBE+U	a=4.464 c=2.955	283.22	-	431.84	113.24	-	209.64	194.34	144.36	-	-	216.85	216.02	277.98	108.05	0.29	2.01
r-CrO ₂	PBEsol+U	a=4.408 c=2.919	302.51	-	482.47	122.24	-	247.08	254.95	171.31	-	-	252.39	245.13	268.17	101.36	0.32	2.49
r-CrO ₂	Expt. [29]	a=4.421 c=2.916												242 ± 2				
o-CrO ₂	PBE+U	a=4.463 b=4.465 c=2.956	272.66	272.60	419.28	116.02	115.98	210.44	197.75	151.11	150.98	-	216.67	193.94	267.48	103.33	0.29	2.10
o-CrO ₂	PBEsol+U	a=4.407 b=4.406 c=2.920	306.76	305.99	460.08	131.78	131.83	238.70	229.74	169.98	169.76	-	244.49	216.75	295.88	113.95	0.30	2.15
o-CrO ₂	Expt. [29]	a=4.425 b=3.987 c=2.683												181 ± 3				
h-CrO ₂	PBE+U	a=9.880 c=2.978	141.33	-	278.19	75.39	-	37.73	119.95	62.77	-	5.93	115.63	111.48	117.54	44.17	0.33	2.62
h-CrO ₂	PBEsol+U	a=9.767 c=2.928	174.89	-	254.52	83.16	-	41.61	100.41	80.16	-	-8.92	124.24	119.01	154.54	59.77	0.29	2.08
h-MnO ₂	PBE+U	a=9.920 c=2.935	139.56	-	309.64	77.66	-	37.75	100.58	58.91	-	12.32	111.01	120.98	131.12	50.31	0.30	2.21
h-MnO ₂	PBEsol+U	a=9.787 c=2.903	148.27	-	331.03	82.05	-	38.25	112.11	66.75	-	13.81	121.11	128.58	131.93	50.03	0.32	2.42
h-MnO ₂	Expt. [59]	a=9.750 c=2.861																

TABLE I. The lattice constants, elastic constants (C_{ij}), bulk moduli (B_H), Young moduli (Y), Sheer moduli (G), Poisson ratios (ν), Pugh ratios (B_H/G) calculated from energy-strain relationship following the formula by Hill [60] and bulk moduli calculated using equation of state proposed by Vinet et. al. [61] (B_V) for rutile (r) and hollandite (h) type CrO₂ and h-MnO₂.

response.

Furthermore, the h-CrO₂ structure has been optimised

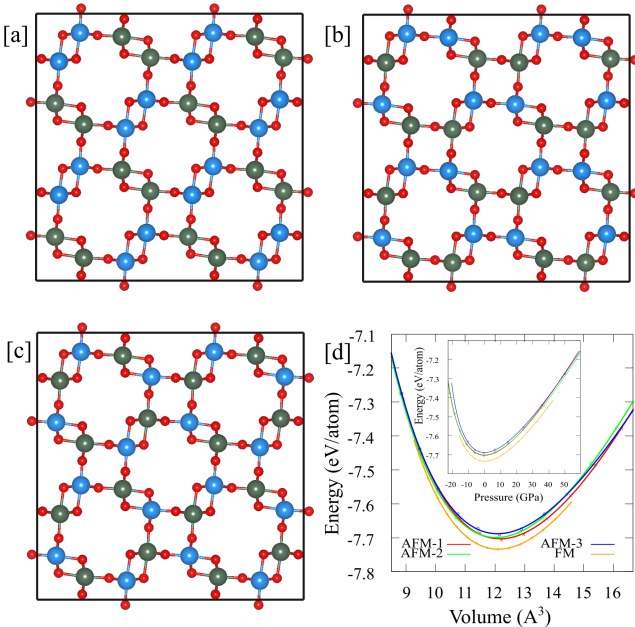


FIG. 3. (a-c) The anti-ferromagnetic spin configurations in a $2 \times 2 \times 1$ supercell of conventional unit cell. Green and blue dots represent atoms with opposite spins. (d) Energy vs. volume and energy vs. pressure (inset) plot for three anti-ferro and the ferromagnetic configurations. The solid lines are the Vinet equation of state fitted curves using the data shown as points [61].

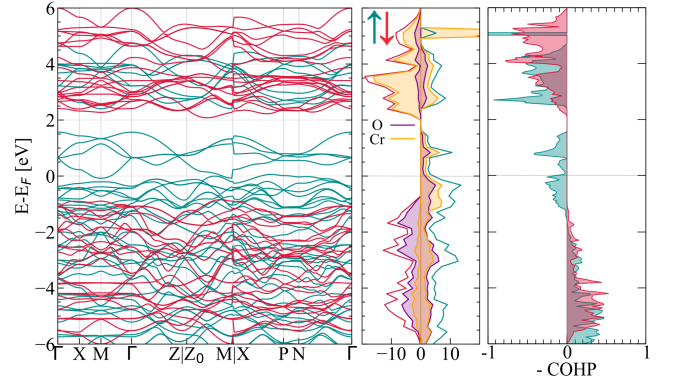


FIG. 4. Energy band diagram, density of states per unit cell, and the negative crystal orbital Hamiltonian populations ($-COHP$) of h-CrO₂ crystal.

using a variation of Hubbard term. Throughout the range of $U - J = 0$ to $U - J = 7$ the FM configuration remains the ground state as depicted in Fig.A.2. The energy variation with $U - J$ is non-linear with low eccentricity. For FM configuration this curvature is highest.

On the other hand, h-MnO₂ which has similar structure is found to be in AFM-3 ground state with the spin distribution as in Fig.3(c) [9, 52]. Interestingly, for h-CrO₂ this AFM-3 configuration possesses the highest energy.

The h-CrO₂ is a ferromagnetic material where the nature of bands for up and down spins are quite different. The metallic nature of one spin (up) is contradicted by the semiconductor nature for the other spin (down) channel making the h-CrO₂ a half-metal. The electronic band dispersion and the density of states (DOS) near the Fermi level (E_F) is depicted

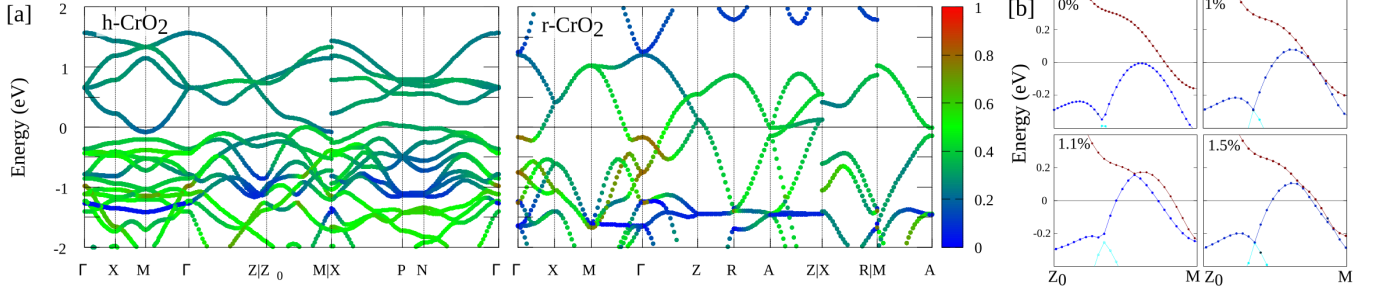


FIG. 5. (a) Percentage contribution from Oxygen orbitals for the bands near Fermi energy of h-CrO₂ and r-CrO₂, (b) Evolution of bands crossing the Fermi energy for h-CrO₂ with uniaxial pressure along z-axis.

in Fig.4. The majority spin bands crosses E_F , while, the down spin channel shows a gap. The half-metallic bandgap is found to be 2.9 eV. There is no state over -0.85 eV and below 2.07 eV relative to E_F in minority spin channel. The half-metallic gap is indirect on the Z_0 –M line of irreducible Brillouin Zone (BZ) edge (see, Fig.A.1). For majority spin channel, in conduction band, first four bands are separated from the others by 0.82 eV from 1.56 eV at Γ to 2.38 eV at M w.r.t. E_F . An interesting feature is that the eigenvalues for all the bands at Z are equal with those at Z_0 , so, the diagonally opposite points of upper surface of the irreducible BZ are equivalent.

The DOS for majority spin channel is shifted lower than the minority spin channel. Shifting of DOS is an well-known sign of ferromagnetic character of material as well as the dissimilarity of DOS represents the ferromagnetic strength. For CrO₂, the dissimilarity is vividly noticeable, so, the found magnetic moment of 2 μ_B per formula unit is quite justified.

Electronic bonding analysis can provide more insight of the ferromagnetic character of h-CrO₂ [70]. For localised basis set the atomic orbital overlap is straight-forward to calculate, so, the overlap population weighted DOS (crystal orbital overlap population, COOP) can provide the information on the nature of bonding, anti-bonding, or non-bonding interaction. For DFT calculation involving plane wave basis, crystal orbital Hamiltonian populations (COHP) is a method that partitions band energies into pairwise atomic orbital interactions facilitating similar identification. There is no anti-bonding state below E_F for down spin, whereas, for up spin, the anti-bonding state starts -1.78 eV. Such extended anti-bonding state is generated from Cr-3d and O-2p interaction which becomes clear from the orbital weighted bands in Fig.A.4. The bonding anti-bonding nature is similar in rutile phase as well (see, Fig.A.3)

To get a closer look on the orbital contribution on the full spaghetti of bands, the orbital weighted bands are plotted in Fig.A.4. The lowest lying bands 40 eV below E_F are originating from the s and p orbitals of Cr, and, the majority spin bands are lower in energy than the minority spin bands. The O-2s bands are also separated below 20 eV. Near E_F , in valence band, the most contribution is coming from the O-2p orbitals. For majority spin channel, the Cr-3d_{xy} bands are separately visible. There is a small electron pocket at M which is visible along X–M– Γ and Z_0 –M line. The pocket is conduced mostly from Cr-3d_{xy} and Cr-3d_{x²-y²}. Also, there is an hole pocket along X–P with most contribution coming from hybridised Cr-3d_{xz} and O-2p_x. The band creating the hole pocket is more flat than the band responsible for electron

pocket indicating heavier hole than electron at E_F .

From the partial DOS plot for Cr and O we have already noticed that the conduction bands are formed by Cr orbitals and the valence bands are mostly coming from O orbitals. Cr and O orbital mixing is better experienced for up spin. Now, r-CrO₂ is understood to be a negative charge transfer gap material [35]. Korotin *et al.* have shown that a almost pure O-2p band crosses the Fermi energy which acts as a electron/hole reservoir causing fractional occupation of Cr-3d band at E_F . In Fig.5(a) we have presented the oxygen weighted bands for both rutile and hollandite structure. In both cases, there is a Cr-3d band below E_F contributing mostly from 3d_{xy} orbital. However, in hollandite structure, it is not as much a separate unhybridised band, so, Cr-3d_{xy} orbital in h-CrO₂ is not as localised as in rutile counterpart. In r-CrO₂, in the vicinity of BZ centre Γ , the band crossing E_F holds its pure O-2p character (brown dots), though hybridizes with Cr-3d near Z. So, hybridisation is much anisotropic in r-CrO₂ for the said band. In h-CrO₂ there are two bands responsible for the metallic character, the band crossing E_F around M has almost pure Cr-3d character and the band crossing along X–P is a hybridised Cr-d_{xz} and O-2p_x band. In both polymorphs, the band mixing between Cr-3d and O-2p is accountable for the half-metallic ferromagnetic character, though, the nature of hybridisation is different.

Magneto-crystalline anisotropy: h-CrO₂ possesses a rare porous hollandite crystal structure and belongs to a scarce ferromagnetic TMO family. It would be interesting to see how the crystal structure tunes the direction of magnetic moment in this system. Magneto-crystalline anisotropy is a phenomenon manifested by the variation of internal energy depending on the direction of magnetization in any material. As the orbit is strongly coupled to the crystal structure (lattice), so, changing the orientation of spin is resisted through spin-orbit coupling giving rise to MAE [71, 72]. The spatial variation of MAE is presented in Fig.6. The three dimensional plot is showing an isotropy in X–Y plane (azimuthal independence). Here to mention that the bulk modulus for this structure has also shown azimuthal symmetry (refer Fig.2(d)). This is a feature of its layered structure. However, tilting the spin through making an angle θ with Z-axis (easy axis) demands external energy. The MAE variation with θ shows that the hardest axis lies on X–Y plane with highest value of $MAE = 394.96 \mu\text{eV}$.

Topological character under uniaxial pressure: Ferromagnetic Weyl materials poised to be integral part of rich Physics [73, 74]. Occurrence of Weyl points in r-CrO₂ has

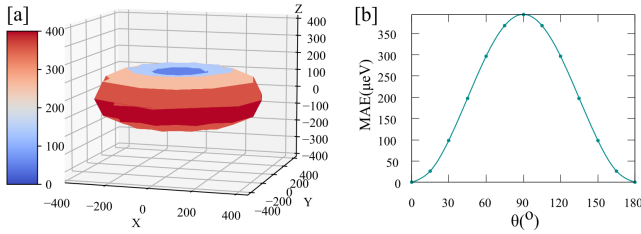


FIG. 6. Magneto-crystalline anisotropic energy (μeV) variation of h-CrO₂ crystal in (a) 3-dimension, and in (b) X-Y plane, where θ is the angle with Z-axis.

been reported recently [39]. As we see in Fig.5, along Z_0 -M near E_F two bands are almost touching each other within ± 0.5 eV range about E_F . Referring to Fig.A.4, we can observe that one of these bands have strong Cr- $3d_{xz}$ contribution and, another with O- $2p_z$ orbital share. This makes us curious if uniaxial pressure along z-axis can bring some fundamental change of band topology (see, Fig.5(b)). With 1% pressure, the bands touches each other. With higher pressure, band inversion feature is observed maintaining the band-topology conserved always. These two bands come close at two points, one above E_F , another below E_F . This is a signature of type-II Weyl material [75]. More comprehensive study on the topological aspect of this material is aimed to be explored in future.

V. CONCLUSION

α -MnO₂ structure is one of its kind with a 2×2 tunnel to accommodate foreign elements which can be found to be useful in different applications. We have predicted another TMO having a similar structure, yet drastically different electronic and magnetic character. Even, it demonstrates interesting mechanical and electronic behaviour compared with other Chromium dioxides. A detailed side-by-side study reveals the underlying Physics of such a vibrant character.

The system is mechanically and dynamically stable. It exhibits anisotropic elastic moduli and is less stiff than the similar h-MnO₂ structure. The lattice parameters and elastic constants calculated for hollandite h-MnO₂ and rutile r-CrO₂ are at par with the experimental values exhibiting the reliability of methodology utilised for the proposed h-CrO₂ crystal.

The h-CrO₂ is a half-metallic ferromagnet having a half-metallic bandgap of 2.9 eV. The ferromagnetic nature is a result of strong hybridisation of Cr- $3d$ and O- $2p$ electrons. The band crossing is minimal with only one electron pocket around M conduced mostly from Cr- $3d_{xy}$ and Cr- $3d_{x^2-y^2}$, and one hole pockets along X-P with most contribution coming from hybridised Cr- $3d_{xz}$ and O- $2p_x$ at Fermi level. The occurrence of electron-hole pocket is at different k-points, so, the direct electron-hole coupling is not possible. However, the prospect of phonon mediated superconductivity is yet to be investigated.

The crystal shows ample magneto-crystalline anisotropy with the easy axis perpendicular to the plane of the structure (Z-axis) with highest value of $MAE = 394.96 \mu\text{eV}$, while the azimuthal angle independence of MAE is evident. Though there are two bands almost touching together near Fermi level, the band topology remains conserved upon uniaxial pressure. However, the transformation of bands near Fermi energy with minimal uniaxial pressure may pave the way for further detailed study on the topological aspects of this material.

To sum up, we can conclude that a new stable transition metal oxide with vibrant physical properties is proposed which may further ignite the interest of Physics community.

ACKNOWLEDGEMENT

The author want to thank Prof. Debnarayan Jana of University of Calcutta, India for enriching discussion and Prof. Sajeev John of University of Toronto, Canada for providing computational facility.

-
- [1] A. Byström and A. M. Byström, Acta Crystallographica **3**, 146 (1950).
 - [2] J. Luo, H. Zhu, J. Liang, G. Rao, J. Li, and Z. Du, The Journal of Physical Chemistry C **114**, 8782 (2010).
 - [3] L. Li, Y. Pan, L. Chen, and G. Li, Journal of Solid State Chemistry **180**, 2896 (2007).
 - [4] X. Gao, H. Wu, W. Li, Y. Tian, Y. Zhang, H. Wu, L. Yang, G. Zou, H. Hou, and X. Ji, Small **16**, 1905842 (2020).
 - [5] S. J. Kim, D. Wu, N. Sadique, C. D. Quilty, L. Wu, A. C. Marschilok, K. J. Takeuchi, E. S. Takeuchi, and Y. Zhu, Small **16**, 2005406 (2020).
 - [6] Z. Hu, X. Xiao, C. Chen, T. Li, L. Huang, C. Zhang, J. Su, L. Miao, J. Jiang, Y. Zhang, *et al.*, Nano Energy **11**, 226 (2015).
 - [7] L.-T. Tseng, Y. Lu, H. M. Fan, Y. Wang, X. Luo, T. Liu, P. Munroe, S. Li, and J. Yi, Scientific reports **5**, 1 (2015).
 - [8] V. Tripkovic, H. A. Hansen, and T. Vegge, ChemSusChem **11**, 629 (2018).
 - [9] E. Cockayne and L. Li, Chemical Physics Letters **544**, 53 (2012).
 - [10] Y. Wang, H. Liu, X. Sun, and I. Zhitomirsky, Scripta Materialia **61**, 1079 (2009).
 - [11] D. Wang, L. Wang, G. Liang, H. Li, Z. Liu, Z. Tang, J. Liang, and C. Zhi, ACS nano **13**, 10643 (2019).
 - [12] R. Zhang, X. Yu, K.-W. Nam, C. Ling, T. S. Arthur, W. Song, A. M. Knapp, S. N. Ehrlich, X.-Q. Yang, and M. Matsui, Electrochemistry Communications **23**, 110 (2012).
 - [13] J. Mondal and S. K. Srivastava, ACS Applied Nano Materials **3**, 11048 (2020).
 - [14] S. Sivakumar and L. N. Prabu, Materials Today: Proceedings **47**, 52 (2021).
 - [15] Y. Dong, J. Zhao, J.-Y. Zhang, Y. Chen, X. Yang, W. Song, L. Wei, and W. Li, Chemical Engineering Jour-

- nal **388**, 124244 (2020).
- [16] W. Abriel, F. Rau, and K.-J. Range, *Materials Research Bulletin* **14**, 1463 (1979).
 - [17] M. Carter, E. Vance, D. Mitchell, J. Hanna, Z. Zhang, and E. Loi, *Journal of Materials Research* **17**, 2578 (2002).
 - [18] O. Lebedev, S. Hébert, V. Roddatis, C. Martin, S. Turner, A. Krashennnikov, Y. Grin, and A. Maignan, *Chemistry of Materials* **29**, 5558 (2017).
 - [19] L. J. V. Stimpson, J. M. Powell, G. B. Stenning, M. Jura, and D. C. Arnold, *Physical Review B* **98**, 174429 (2018).
 - [20] T. Endo, S. Kume, N. Kinomura, and M. Koizumi, *Materials Research Bulletin* **11**, 609 (1976).
 - [21] H. Okada, N. Kinomura, S. Kume, and M. Koizumi, *Materials Research Bulletin* **13**, 1047 (1978).
 - [22] M. Isobe, S. Koishi, N. Kouno, J.-I. Yamaura, T. Yamauchi, H. Ueda, H. Gotou, T. Yagi, and Y. Ueda, *Journal of the Physical Society of Japan* **75**, 073801 (2006).
 - [23] K. Hasegawa, M. Isobe, T. Yamauchi, H. Ueda, J.-I. Yamaura, H. Gotou, T. Yagi, H. Sato, and Y. Ueda, *Physical review letters* **103**, 146403 (2009).
 - [24] O. Tamada, N. Yamamoto, T. Mori, and T. Endo, *Journal of Solid State Chemistry* **126**, 1 (1996).
 - [25] P. Mahadevan, A. Kumar, D. Choudhury, and D. Sarma, *Physical review letters* **104**, 256401 (2010).
 - [26] T. Toriyama, A. Nakao, Y. Yamaki, H. Nakao, Y. Murakami, K. Hasegawa, M. Isobe, Y. Ueda, A. Ushakov, D. Khomskii, *et al.*, *Physical Review Letters* **107**, 266402 (2011).
 - [27] I. Pirrotta, J. Fernández-Sanjulián, E. Moran, M. Alario-Franco, E. Gonzalo, A. Kuhn, and F. García-Alvarado, *Dalton Transactions* **41**, 1840 (2012).
 - [28] P. Marcus, S. Qiu, and V. Moruzzi, *Journal of Physics: Condensed Matter* **10**, 6541 (1998).
 - [29] B. Maddox, C. Yoo, D. Kasinathan, W. Pickett, and R. Scalettar, *Physical Review B* **73**, 144111 (2006).
 - [30] A. Y. Kuznetsov, J. De Almeida, L. Dubrovinsky, R. Ahuja, S. Kwon, I. Kantor, A. Kantor, and N. Guignot, *Journal of applied physics* **99**, 053909 (2006).
 - [31] H. Bendaoud, K. Obodo, and B. Bouhafs, *Computational Condensed Matter* **21**, e00400 (2019).
 - [32] S. Kim, K. Kim, C.-J. Kang, and B. Min, *Physical Review B* **85**, 094106 (2012).
 - [33] S. Huang, X. Wu, J. Niu, and S. Qin, *RSC advances* **8**, 24561 (2018).
 - [34] K. Schwarz, *Journal of Physics F: Metal Physics* **16**, L211 (1986).
 - [35] M. Korotin, V. Anisimov, D. Khomskii, and G. Sawatzky, *Physical Review Letters* **80**, 4305 (1998).
 - [36] M. Katsnelson, V. Y. Irkhin, L. Chioncel, A. Lichtenstein, and R. A. de Groot, *Reviews of Modern Physics* **80**, 315 (2008).
 - [37] E. Kulatov and I. Mazin, *Journal of Physics: Condensed Matter* **2**, 343 (1990).
 - [38] J. Zaanen, G. Sawatzky, and J. Allen, *Physical review letters* **55**, 418 (1985).
 - [39] R. Wang, Y. Jin, J. Zhao, Z. Chen, Y. Zhao, and H. Xu, *Physical Review B* **97**, 195157 (2018).
 - [40] D. A. Tompsett and M. S. Islam, *Chemistry of Materials* **25**, 2515 (2013).
 - [41] L. Li, C. Nan, J. Lu, Q. Peng, and Y. Li, *Chemical communications* **48**, 6945 (2012).
 - [42] J. J. Attema, L. Chioncel, C. Fang, G. A. de Wijs, and R. de Groot, *Local-Moment Ferromagnets: Unique Properties for Modern Applications*, 199 (2005).
 - [43] V. Y. Irkhin and M. I. Katsnel'son, *Physics-Uspekhi* **37**, 659 (1994).
 - [44] S. Yuasa, K. Hono, G. Hu, and D. C. Worledge, *MRS Bulletin* **43**, 352 (2018).
 - [45] D. A. Keen, *Journal of Physics: Condensed Matter* **14**, R819 (2002).
 - [46] B. Himmetoglu, A. Floris, S. De Gironcoli, and M. Cococcioni, *International Journal of Quantum Chemistry* **114**, 14 (2014).
 - [47] G. Kresse and J. Furthmüller, *Physical review B* **54**, 11169 (1996).
 - [48] J. P. Perdew, K. Burke, and M. Ernzerhof, *Physical Review Letters* **78**, 1396 (1997).
 - [49] J. P. Perdew, A. Ruzsinszky, G. I. Csonka, O. A. Vydrov, G. E. Scuseria, L. A. Constantin, X. Zhou, and K. Burke, *Physical review letters* **100**, 136406 (2008).
 - [50] E. Şaşıoğlu, C. Friedrich, and S. Blügel, *Physical Review B* **83**, 121101 (2011).
 - [51] W. Pickett, S. Erwin, and E. Ethridge, *Physical Review B* **58**, 1201 (1998).
 - [52] B. Paul, D. Mondal, D. Bhattacharya, S. Datta, M. Kundu, I. Mondal, P. Halder, S. Sarkar, A. Ghosh, T. Mandal, *et al.*, *Chemical Engineering Journal* **459**, 141560 (2023).
 - [53] K. Momma and F. Izumi, *Journal of Applied crystallography* **41**, 653 (2008).
 - [54] S. Yalameha, Z. Nourbakhsh, and D. Vashae, *Computer Physics Communications* **271**, 108195 (2022).
 - [55] V. Wang, N. Xu, J.-C. Liu, G. Tang, and W.-T. Geng, *Computer Physics Communications* **267**, 108033 (2021).
 - [56] R. Nelson, C. Ertural, J. George, V. L. Deringer, G. Hautier, and R. Dronskowski, *Journal of Computational Chemistry* **41**, 1931 (2020).
 - [57] H. Miura, *Mineralogical Journal* **13**, 119 (1986).
 - [58] S. Sun, X. Zhang, J. Cui, Q. Yang, and S. Liang, *Nanoscale* **11**, 15739 (2019).
 - [59] Z. Chen, Z. Jiao, D. Pan, Z. Li, M. Wu, C.-H. Shek, C. L. Wu, and J. K. Lai, *Chemical Reviews* **112**, 3833 (2012).
 - [60] R. Hill, *Proceedings of the Physical Society. Section A* **65**, 349 (1952).
 - [61] P. Vinet, J. Ferrante, J. Smith, and J. Rose, *Journal of Physics C: Solid State Physics* **19**, L467 (1986).
 - [62] M. Born, K. Huang, and M. Lax, *American Journal of Physics* **23**, 474 (1955).
 - [63] F. Mouhat and F.-X. Coudert, *Physical review B* **90**, 224104 (2014).
 - [64] W. Voigt, Teubner, Leipzig (1928).
 - [65] A. Reuß, *ZAMM-Journal of Applied Mathematics and Mechanics/Zeitschrift für Angewandte Mathematik und Mechanik* **9**, 49 (1929).
 - [66] P. Vinet, J. Ferrante, J. H. Rose, and J. R. Smith, *Journal of Geophysical Research: Solid Earth* **92**, 9319 (1987).
 - [67] H. Wu, Y. Chen, C. Deng, and X. Su, *Phase Transitions* **85**, 708 (2012).
 - [68] Y. Li and J. Hao, *Solid state communications* **152**, 1216 (2012).
 - [69] S. Alptekin, *Journal of molecular modeling* **21**, 1 (2015).
 - [70] R. Dronskowski, *International journal of quantum chemistry* **96**, 89 (2004).
 - [71] G. Daalderop, P. Kelly, and M. Schuurmans, *Physical Review B* **41**, 11919 (1990).

- [72] D. Sander, Journal of Physics: Condensed Matter **16**, R603 (2004).
- [73] M. Kanagaraj, J. Ning, and L. He, Reviews in Physics **8**, 100072 (2022).
- [74] Q. Wang, Y. Xu, R. Lou, Z. Liu, M. Li, Y. Huang, D. Shen, H. Weng, S. Wang, and H. Lei, Nature communications **9**, 3681 (2018).
- [75] B. Yan and C. Felser, Annual Review of Condensed Matter Physics **8**, 337 (2017).

Appendix:

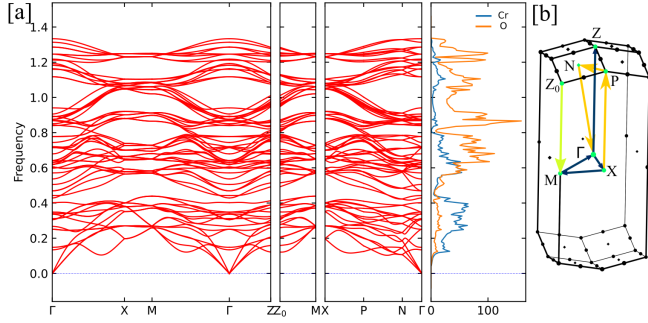


FIG. A.1. (a) Phononic band structure and DOS of h-CrO₂; (b) The irreducible Brillouin zone and the k-path selected for band structure.

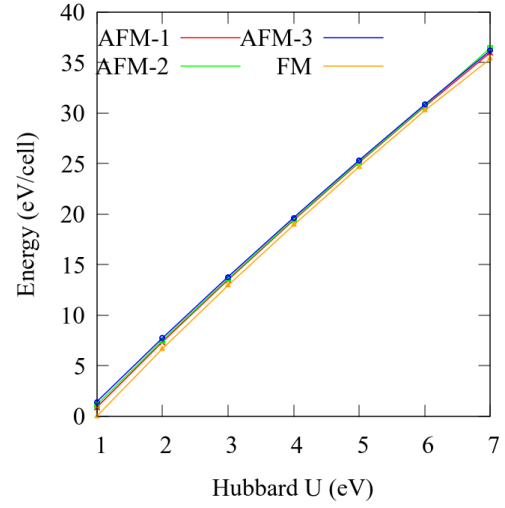


FIG. A.2. Total energy w.r.t. ground state energy per unit cell for different magnetic configurations of h-CrO₂.

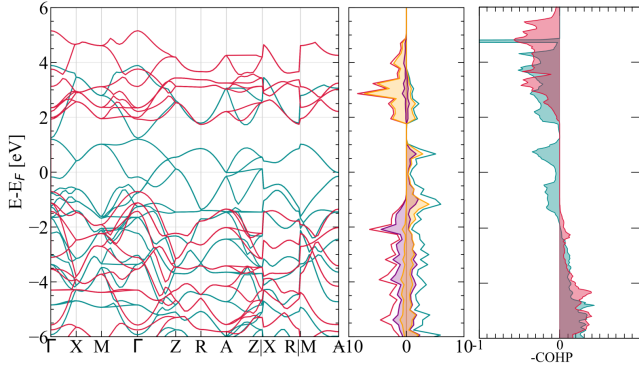


FIG. A.3. Energy band diagram, density of states, and the negative crystal orbital Hamiltonian populations ($-\text{COHP}$) of $r\text{-CrO}_2$ crystal.

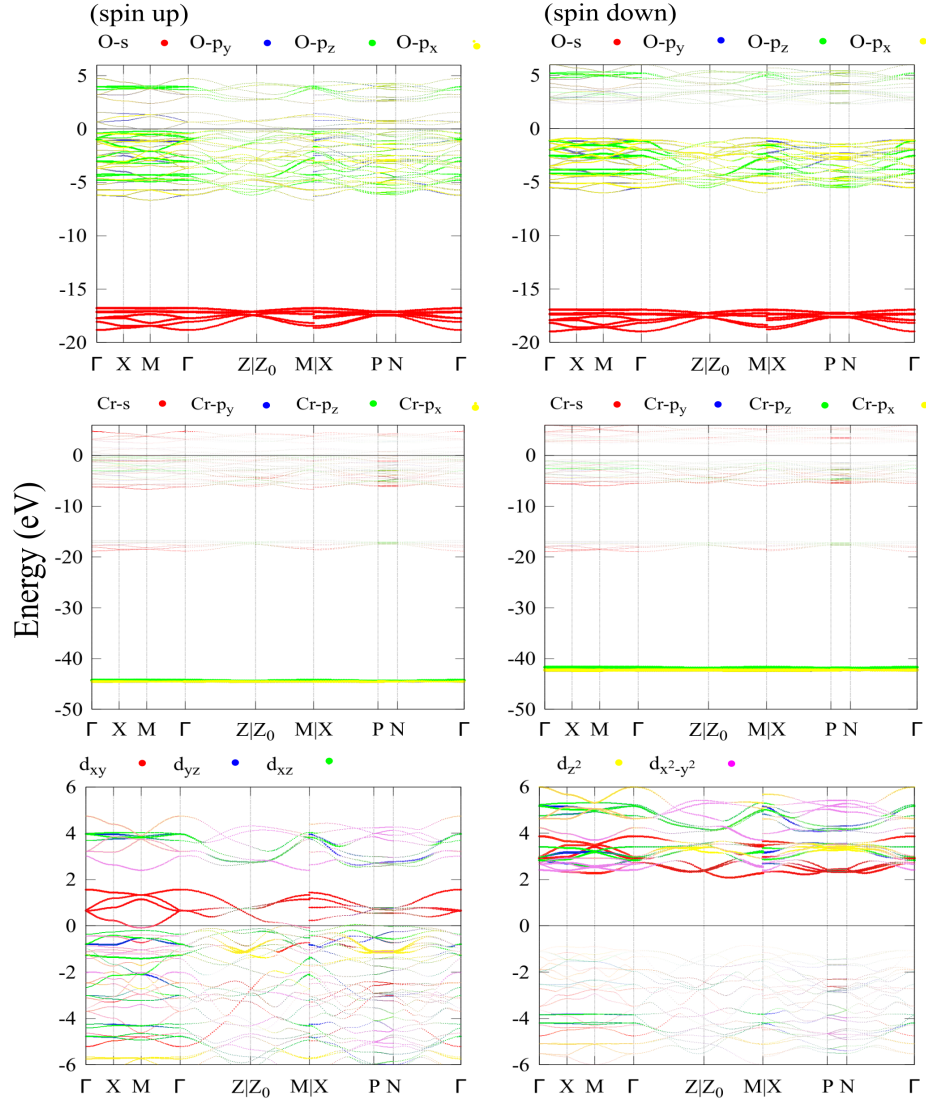


FIG. A.4. Orbital weighted band dispersion of $h\text{-CrO}_2$.